Robust time-lapse *AVOA* analysis using *OBC*: a case study from Teal South

Asghar Shams and Colin MacBeth, Heriot-Watt University, Edinburgh, UK*

Summary

A methodology is developed for pre-stack processing of time-lapse *P*-wave seismic to preserve the azimuthal anisotropy signature in a robust and controlled fashion. The approach is applied to *P-Z* summed *OBC* data from the Teal South field, Gulf of Mexico. A new technique based on polarization filtering is then used to preferentially separate the anisotropy from the geology response. This process reveals discrete anomalies distributed on or around a turbidite sand body. These anomalies change intensity before and after production, with their position and orientation coinciding with the high net-to-gross sands. This observation is consistent with known turbidite depositional models.

Introduction

The Teal South *4D-4C* project managed by the Energy Research Clearing House in Houston provides a unique opportunity to study the benefits of monitoring time-lapse variations in azimuthal anisotropy using both *P-S* (Entralgo and Spitz 2001) and *P-P* data. Such work complements land multi-component (*S-S*) studies for azimuthal anisotropy (Angerer et al. 2000). It is anticipated that observations of anisotropy could prove useful in discriminating between the effects of pressure/stress and saturation, and detecting dynamic changes in the reservoir properties of fractured or faulted reservoirs. Azimuthal anisotropy could be of particular benefit in situations where the stack or *AVO* response is unable to resolve major controlling elements for quantitative reservoir description.

Time-lapse anisotropy offers an additional set of measurements with which to constrain our understanding of the current *4D* signature on Teal South (Pennington et al. 2001) and the history match (Christie et al. 2002). However to deliver a credible update to the reservoir model, it is essential that the extracted anisotropy and time-lapse signature should be robust and the impact of the noise floor understood. Thus, our approach is to develop a processing scheme and new interpretation algorithms to extract the seismic anisotropy signature with minimal artifacts and quality control at each step of the process. For the purposes of this work we focus on the azimuth and offset variations of the *P-P* amplitude, developing new analysis algorithms, and thus extending an earlier study by Hall and MacBeth (2001).

Datasets and pre-stack processing flow

The data considered are taken from Phase I and Phase II ocean bottom cable (OBC) surveys of the Teal-South experiment shot in the Gulf of Mexico. Phase I was shot in July 1997 with four E-W oriented cables spaced 400m apart. There are six receivers in each cable, arranged at a 200m interval. The shot point grid is at 25m increments in both the in-line and cross-line direction, and distributed over an area of 3x3km^2. Phase II was shot in April 1999 with identical receiver parameters but three N-S lines of four receivers are added to the east of the original lines. The shot point spacing is the same as before but the area covered is now approximately 4x3km^2. The reservoir target of interest in this current work is a thin turbidite sand located at 4500 ft and between two faults visible at the seismic

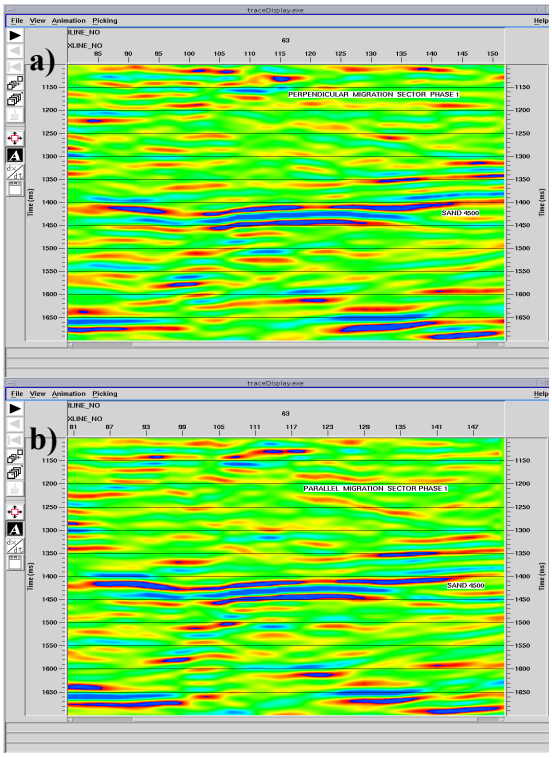

Figure 1: Inline-No 63 of Phase I. Final migrated sections a) Perpendicular sector b) Parallel sector. Notice that there is a good similarity between the above sections and the minor differences are related to anisotropy.

scale. The *OBC* provide the wide azimuth and offset coverage necessary for *AVOA* studies and true *3D* imaging. However this particular acquisition geometry creates a patchy distribution of offset and azimuth that prevents straightforward analysis. Due to this condition we choose to follow the restricted-azimuth approach (Lynn et al. 1996) in order to boost the fold at each offset for each single CMP. Thus, the data are sorted into two azimuth sectors centered on directions parallel and perpendicular to a prescribed principal direction, which in this case is not necessarily attributed to fractures or stress. To maximize our return, a pre-stack processing flow is constructed to focus on preservation of both the time-lapse and azimuthal anisotropy signature. The processing is achieved by developing a method for parallel pre-stack restricted azimuth processing (PRAP). The main steps of this processing approach are: 1) relative amplitude preservation; 2) removal of acquisition artifacts (offset-azimuth balancing, source and receiver consistency, source directivity, acquisition direction) and geometric phase balancing; 3) removal of processing artifacts (migration effects, multiples, dip effects, binning, velocity analysis direction), combined with amplitude and frequency balancing.

To begin with we divide each dataset into two sectors parallel and perpendicular to the principal field direction in the Teal-South. This is based on previous studies of the *P-S* data (Entralgo and Spitz 2001) and also the original trend of two main faults; the estimated orientation is N15E. Each sector is defined by 55 degrees either side of N15E and N75W. The datasets are then moved through the processing, being treated individually but also simultaneously. Figure 1 shows two vertical sections across the 1997 volume, to illustrate the reduction in noise levels and artifacts achieved. After application of a post-stack cross-matching scheme between the Phase I and Phase II datasets, the time-lapse anisotropy signature is revealed. To further verify the results, a different limited azimuth set (E-W and N-S) are also processed with similar conclusions.

Anisotropy enhancement technique

Maps of *RMS* amplitude over a horizon slice picked to run through the 4500' sand are produced for each of the two surveys and for the 'fracture' parallel and perpendicular sectors (Figure 2). These four maps are now further processed to extract the magnitude and orientation of the anisotropy signature. For each survey the amplitudes, R_{par} and R_{perp} can be represented by:

$$R_{par} = G + A_{par} + N_1 \qquad (1)$$

and

$$R_{perp} = G + A_{perp} + N_2 \qquad (2)$$

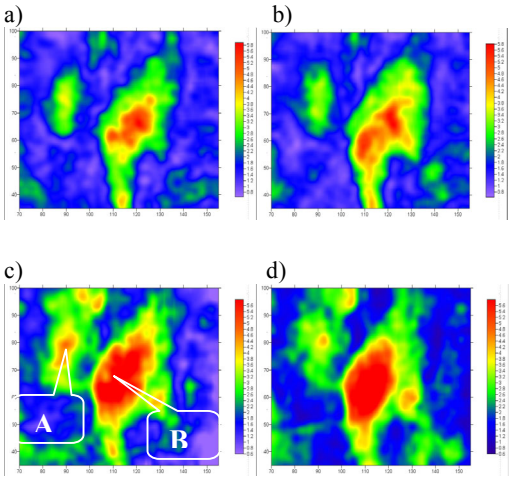

Figure 2. Maps of *RMS* amplitude across the horizon slice for the 4500' sand. Phase I (1997): a) parallel sector; b) perpendicular sector. Phase II (1999): c) parallel sector; d) perpendicular sector. A brightening has occurred on Phase II related to increasing gas saturation in main reservoir (labeled B) due to production. In Phase II (c and d) the 'little neighbor' reservoir (Pennington et al. 2001) (labeled A) becomes visible. Note that many of these are amplitude effects and are not observed in the seismic anisotropy maps of Figure 5.

where G is the geological signal, A_{par} and A_{perp} are the anisotropy signature determined by both the magnitude of the anisotropy and the orientation of the principal axes, and finally N_1 and N_2 are random noise fields. A filter based on polarization filtering of *3C* data (MacBeth 2002) is developed for separating anisotropy and geology effects in the presence of noise. Figure 3 illustrates this filter, where 'fracture' parallel (u) and perpendicular (v) data are cross-plotted. As the data have been balanced during the processing, points which lie on the line u=v are related to the geology signal, whilst the off-diagonal points relate to anisotropy or the random noise. The polarization filter is designed to preferentially select either the geology or the anisotropy. The filter is applied as spatially-dependent weights to both RMS amplitude maps, with the weights being a function of the cosine of the angle, ψ, between the ideal geology vector (1,1) and the actual result (u, v). After separation, the magnitude and direction of the anisotropy can be computed according to projection geometry.

Interpretation of *4D AVOA* anomalies

On the *P-P* stack response there is a clear amplitude brightening observed in Phase II due to gas emanating from

solution. This brightening occurs at the same time for both the main sand body and the 'little neighbor', which are connected via sands to the North. Much of the anisotropy response (Figure 5) is independent of these bright areas and quite different in character. Indeed, for the majority of the reservoir and its surroundings the magnitude of the anisotropy is virtually zero, consistent with the notion that the unconsolidated sands cannot support fractures, and that stress-induced azimuthal anisotropy is unlikely as the area

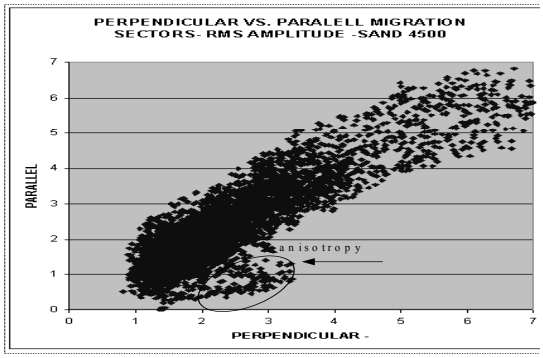

Figure 3. Cross-plot of perpendicular (u) against parallel (v) amplitudes for Phase II. All points clustered around u=v are related to the isotropic (geology) response, and the rest are related to either anisotropy or random noise. A cluster can be observed in the lowest part of cross-plot whose origin is identified as anisotropy.

is not subject to large differential stresses and the drop in pore pressure is small: (from 2820psi at the time of Phase I to 2190psi at Phase II). However, rising above the low anisotropy background are observed five discrete anomalies all varying with production, with orientations on average N32E. The four anomalies lying in the main sand body are distributed and oriented almost exactly along the axis of the cleanest sands as defined by the stack amplitudes on the legacy towed streamer data (Figure 4). There appears to be no correlation with the gas cap which forms up-dip close to well D10 and along the fault to the east. Anisotropy increases are also observed for anomalies 3 and 4, which lie close to the oil-water contact, whilst anomaly 2 lying near well D8 decreases in intensity. The final anomaly, 5, is associated with the 'little neighbour', for which the anisotropy response increases at the gas cap observed in Phase II.

The pattern of anomalies 1, 3 and 4 suggest that the anisotropy is correlated to high porosity and permeability pathways along the regions of clean sand. Due to the link with the high net-to-gross sands (Figure 4), a likely origin is an underlying fabric of alignment related to the direction in which the turbidite flow has been laid down, this imparting a directionality on the individual grains and pore structure. Support for this explanation comes from grain fabric studies from turbidite outcrops and flume tank experiments (Arnott and Hand 1989), which show that sand deposited from turbidity currents have strong grain fabrics with grain long axes parallel to flow and imbricate up-current. The fabric controls the position and orientation of the anisotropy, whilst the seismic visibility is determined by saturation. Calculations based on MacBeth (2001) show that replacement of oil by gas, or oil by brine can enhance existing *P-P AVOA*. The presence of gas could thus explain 5, whilst an explanation for 1, 3 and 4 could be that they are near to the OWC.

Conclusions

P-wave data from a *4D OBC* survey have been analysed for seismic anisotropy. This is achieved by careful processing to preserve the azimuthal signature combined with a new interpretation algorithm. Five distinct anisotropy anomalies are observed on or around the 4500' sand, all of which change with production. These anomalies are distributed along the highest concentration of sand pay, and could be a consequence of turbidite grain fabric and pore structure alignment combined with fluid saturation changes. This information has the potential to radically change the reservoir simulation model.

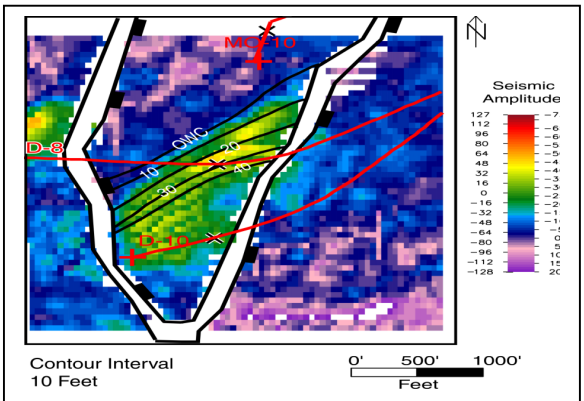

Figure 4. Net pay map of 4500' sand from streamer 1995 survey (Flemings 2000, ERCH Consortium Meeting).

Acknowledgements

We acknowledge Enterprise Oil for a studentship and also support from NIOC. We would also like to thank the Energy Research Clearing House (ERCH) and its sponsors for access to its *4D-4C* Teal South dataset. This project contributes towards the GEOFRAC and ETLP projects at Heriot-Watt University.

References

Arnott, R.W.C., and Hand, B.M., 1989. Bedforms, primary structures and grain fabric in the presence of suspended sediment rain, Journal of Sedimentary Petrology, 59, No.6, 1062-1069.

Angerer, E., Crampin, S., Li, X., and Davis, T., 2000. Time-lapse analysis and detection of fluid changes at Vacuum field, New Mexico, 70th Ann. Internat. Mtg. Soc. Expl. Geophys, 1532-1535.

Christie, M., MacBeth, C., and Subbey, S., 2002. Multiple history-matched models for Teal South, The Leading Edge, 21, 286-289.

Entralgo, R., and Spitz, S., 2001. The challenge of permanent *4C* seafloor systems, The Leading Edge, 20, 614-620.

Hall, S., and MacBeth, C., 2001. *4D-4C AVOA* at the Teal South, 63rd Mtg.Eur.Assn. of Explr. Geophys. session F-22.

Lynn, H. B., Simon, K. M., Bates, C. R. and van Dok, R., 1996. Azimuthal anisotropy in *P*-wave *3-D* (Multiazimuth) data, The Leading Edge, 15, 923-928.

MacBeth, C., 2001. Using *P*-wave data to distinguish gas from water in fractures, Geophysics On-line publication.

MacBeth, C., 2002. Multi component VSP analysis for applied seismic anisotropy, Handbook of Exploration Geophysics, Volume 26, Pergamon.

Pennington, W.D., Acevedo, H., Haataja, J. I. and Minaeva, A., 2001. Seismic time-lapse surprise at Teal South: That little neighbor reservoir is leaking!, The Leading Edge, 20**,** No. 10, 1172-1175.

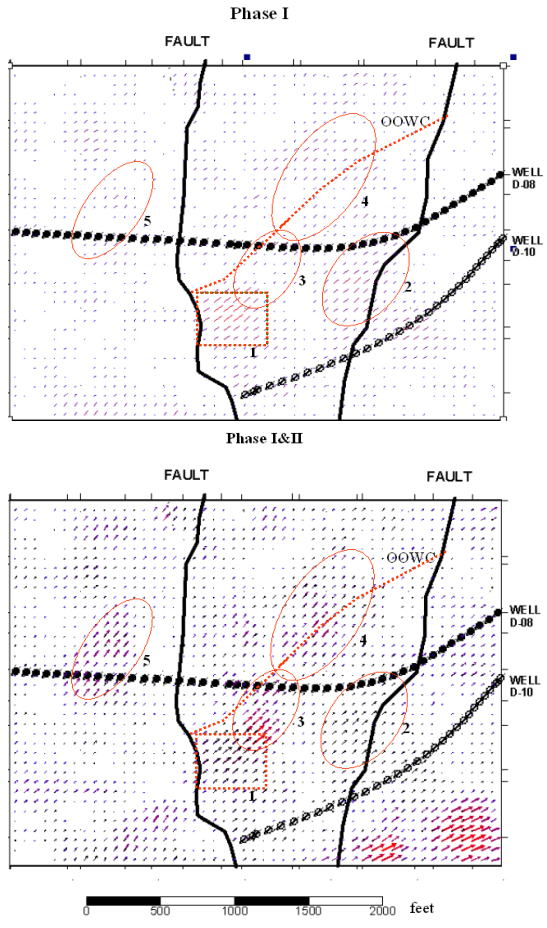

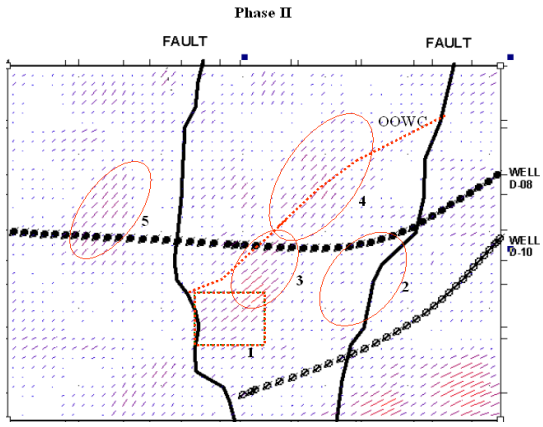

Figure 5: Maps of magnitude and orientation of anisotropy corresponding to Phase I (1997) and Phase II (1999) OBC surveys. Well trajectories and predicted oil-water contact are shown for reference. The overall magnitude of the anisotropy is close to zero in almost all parts of the reservoir, as would be expected for an unconsolidated sandstone. However several discrete time-lapse and seismic anisotropy anomalies can be identified (labeled 1 to 5). Anomalies 3, 4 and 5 increase their intensity with time, whilst anomaly 2 lying close to the penetration point of well D8 decreases in intensity and anomaly 1 remains stable. Anomaly 5 is associated with the little neighbor of Pennington et al. (2001) and is associated with a gas cap. The gas cap up-dip in the main reservoir does not appear to correlated with the anisotropy. The result on the lower right has been identified as processing noise. The thin dotted line is the oil-water contact at Phase I (defined here as the OOWC).